Polyhedron xxx (xxxx) 117027

Contents lists available at ScienceDirect

Polyhedron

journal homepage: www.elsevier.com/locate/poly

Mechanistic investigation of iron-catalyzed cross-coupling using sterically encumbered β-diketonate ligands

Steven J. Scappaticci, Aaron S. Crossman, Alec T. Larson, Franklin D.R. Maharaj, Eser S. Akturk, Michael P. Marshak *

Renewable and Sustainable Energy Institute, University of Colorado Boulder, Boulder CO 80303, United States

ARTICLE INFO

Dedicated to Professor Peter T. Wolczanski on the occasion of his 70th birthday.

Keywords:
acac
Iron
cross-coupling

ABSTRACT

Iron β-diketonate compounds are reported using the hindered 2,6-dimesitylbenzoyl pinacolone (^{Ar}acac), which sterically precludes formation of tris-^{Ar}acac complexes. Fe(^{Ar}acac)$_2$ (**1**), Fe(^{Ar}acac)$_2$Cl (**2**) were synthesized and characterized using crystallographic, spectroscopic, elemental analysis, and electrochemical techniques. Iron complexes with only one ^{Ar}acac ligand form dimers [Fe(^{Ar}acac)(THF)$_2$]$_2$(μ-OTf)$_2$ (**3**) and [(^{Ar}acac)Fe(μ-mesityl)]$_2$ (**4**). Complexes **1**–**4** were evaluated in a Kumada cross-coupling reaction and compared with the parent Fe^{III}(acac)$_3$ complex. Whereas the bis-acac complexes **1** and **2** show only modest activity (~50 % yield after 60 min), the mono-acac complexes **3** and **4** are nearly as effective as the parent compound (~90 % yield). DFT computations, in conjunction with catalytic results and electrochemical observations, suggest a catalytic cycle involving an oxidative addition of an aryl-chloride to Fe(II) to produce a high-spin Fe(IV) complex that could alternately be described as a high-spin Fe(II) stabilizing two coordinated organoradicals. These results suggest that a unique aspect of acac as a ligand for this reaction is its ability to support high-spin organoiron complexes, which can provide low-barrier pathways for C–Cl bond cleavage and C—C bond formation reactions.

1. Introduction

Cross-coupling reactions involving Grignard nucleophiles iron catalysts were among the first cross coupling reactions investigated and predate the more popular palladium catalysis by a few years [1–3]. These reactions occur at low temperatures (0 °C or below) and with short reaction times, often ranging from 5 to 20 min. The promise of having reactions catalyzed by a benign transition metal under mild conditions and short reaction times is tantalizing, which begs the question: why has iron-catalyzed cross-coupling not usurped palladium or nickel as the transition metal of choice in transition metal catalysis? [4].

While these reactions demonstrate the promise of iron-catalysis, the scope of iron-catalyzed cross-coupling remains small [5]. Literature examples of iron-catalyzed Kumada cross-couplings have demonstrated that slight changes in R-groups of electrophiles and nucleophiles result in large variations in yield [6,7]. The blame is laid upon a lack of understanding of the mechanism by which cross-coupling is achieved, leading to a "scattergun" approach to determining whether iron precatalysts are suitable for any given task [8].

Mechanistic investigations of iron-catalyzed Kumada-coupling reactions has led to a wide variety of proposed mechanisms. The initial mechanism proposed by Kochi et. al. in 1974 proposed an Fe(I)/Fe(III) redox manifold, going through a mechanism reminiscent of palladium-catalyzed cross-coupling [9]. This mechanism omitted the ligand, leaving the metalation of ligands on the iron compound in question. Fürstner in 2008 proposed an Fe(–II)/Fe(0) reaction manifold after the isolation of an iron/lithium cluster formed by reacting iron with methyl and ethyl Grignard reagents [10]. By the authors own admission, however, Fe(I)/Fe(III) and Fe(0)/Fe(II) manifolds cannot be excluded as possible mechanisms. Mechanistic investigation in the past 10 years has been predominantly done using iron supported by *N*-heterocyclic carbene and phosphine ligands [11–14]. In these studies, two catalytic cycles utilizing radicals are often posited. In one, an organoiron(II) complex undergoes a single electron transfer reaction to an alkyl chloride. An alkyl radical then adds to the iron center, generating an Fe^{IV} center, which then undergoes reductive elimination to produce cross-coupled product and an iron that must undergo two transmetalation steps to generate the organoiron(II) again. Neidig et. al. proposes a catalytic cycle proposes an Fe(II)/Fe(III) mechanism, utilizing a similar outer sphere radical transfer reaction, but with the alkyl radical never formally binding to the iron center. The authors conclude a review of this mechanistic investigation by stating that "there is no reason to believe

* Corresponding author.
E-mail address: michael.marshak@colorado.edu (M.P. Marshak).

https://doi.org/10.1016/j.poly.2024.117027
Received 1 January 2024; Accepted 10 May 2024
0277-5387/

that all iron–ligand cross-coupling systems undergo a conserved mechanism in the fields of bisphosphines and NHCs" [15]. It is not unreasonable to assert that this logic can similarly be applied to the usage of β-diketonate supported iron catalysts.

Mechanistic investigation of iron-catalyzed Kumada coupling supported by acac ligands have been limited by the inability to sterically control the coordination of acac to iron.The purported purpose of acac ligands is to solubilize the iron center, before other ligands are introduced. Some work has been done utilizing the nitrogen containing cousins to β-diketonates, the β-diketiminate, or "NacNac" ligands. In work published in 2009, Holland et. al. utilized a sterically encumbered NacNac ligand in an effort to investigate the potential role NMP has on iron-catalyzed Kumada cross-coupling [16]. Low valent iron species mono supported by NacNac ligands were isolated, and their catalytic competency was tested against parent $Fe(acac)_3$. It was observed that iron supported by NacNac ligands are not as catalytically active as parent $Fe(acac)_3$. Whether this was due to the steric or electronic effects of the ligand, as well as the identity of the active iron species, were left as open-ended questions.

Utilizing a methodology inspired by Holland et. al., our group has developed a number of acac ligands substituted with sterically bulky *m*-terphenyl groups [17], which we have shown to limit only two ^{Ar}acac to coordinate to M^{3+} [18–24]. By doing so we aimed to isolate similar low-valent iron complexes, and investigate if the electronic structure imparted upon iron by acac ligands was key to achieving an effective pre-catalyst. Alternatively, the bulk of these ligands could enable us to study *in situ* speciation of the active iron species, giving more insight into the catalytically active iron species.

2. Materials and methods

2.1. General methods

Syntheses were performed in a nitrogen-filled glovebox or in a fume hood using standard air-free Schlenk techniques. Organic reagents were purchased from Alfa Aesar, TCI Chemical, or Sigma Aldrich and used as received. $Fe(Mes)_2$ was prepared according to literature procedure and collected and stored at − 30 °C [25]. All solvents were purchased in anhydrous form from Sigma Aldrich and further dried with and stored over 4 Å molecular sieves. Deuterated solvents were purchased from Cambridge Isotope Labs. ^{Mes}ArCOOH [26] and potassium pinacolone enolate [27] were prepared according to literature procedures. NMR spectra were recorded on a Bruker Avance-III 300 NMR spectrometer (300 MHz). IR spectra were recorded on an Agilent Cary 630 FTIR with ATR attachment, UV–vis were recorded on an Avantes AVaSpec-2048L spectrophotometer using a 10 ms integration time and an average of 128 scans per spectrum. Gas chromatography was performed on a ThermoScientific Trace 1310 and mass spectrometry data was collected on an ThermoScientific ISQ LT mass spectrometer. Data was analyzed using Chromeleon 7 software. The concentrated reaction solutions were diluted in 10 mL of hexanes. An aliquot was then diluted tenfold (m/m) in hexanes. Magnetic data were collected in benzene solutions at room temperature using Evans' method [28]. The reported value is the mean of three separately prepared and measured solutions with the standard deviation reported in parenthesis. Magnetic susceptibility data were corrected for diamagnetic contributions for the core diamagnetism of each sample (estimated using Pascal's constants). Elemental Analyses were performed by Midwest Microlab LLC. Cyclic Voltammetry was performed using a Gamry Interface 1000B Potentiostat, using 0.1 M $TBAPF_6$ as a supporting electrolyte. All scans were recorded at 100 mV s^{-1} and voltage calibrated against a ferrocene standard, performed upon the completion of each experiment. X-ray crystal structures were Bruker D8 Quest Eco three circle goniometer platform equipped with a Bruker APEX-II CCD detector. A graphite monochromator was employed for wavelength selection of the Mo Kα radiation (λ = 0.71073 Å). The data were processed using APEX III software provided by Bruker. Except as noted below, structures were solved by intrinsic phasing in SHELXT [29] and refined by standard difference Fourier techniques with SHELXL [30] within the OLEX2 [31] software package. Hydrogen atoms were placed in calculated positions using the standard riding model and refined isotropically.

2.2. Synthesis and characterization of $Fe(^{Ar}acac)_2$ (1)

A 350 mL bomb flask containing a PTFE-coated, magnetic stir bar was charged with 0.240 g of anhydrous $FeCl_2$ (1.88 mmol), 2.000 g of ^{Ar}Acac-K (4.18 mmol) and 100 mL of toluene. The mixture was heated at 150 °C for at least 24 h. After cooling, the mixture was filtered to remove unreacted $FeCl_2$. The filtrate's solvent was removed in vacuo, resulting in an orange solid. Hexanes were added to the solid to selectively precipitate **1** as an orange powder. This suspension was filtered and dried and the powder was collected to yield 0.977 g (50 %) of **1**. IR (solid in Parabar 10,312 oil, cm^{-1}): 1520 (s), 1352 (vs), 850 (s), 767 (m), 678 (m), 491 (w). UV – vis (PhMe): λ_{max} (ε) 454 nm (1630 M^{-1} cm^{-1}), 302 nm (22200 M^{-1} cm^{-1}). Anal. Calcd for $FeC_{62}H_{70}O_4$: C, 79.64; H, 7.57; Found: C, 79.32; H, 7.57.

Crystals of **1-THF$_2$** were obtained by dissolving 50 mg (0.053 mmol) of **1** in 3 mL of THF and 1 mL of toluene, followed by slow evaporation of the solvent under a nitrogen atmosphere. A molecule of toluene was disordered in the crystal lattice. IR (solid in Parabar 10,312 oil, cm^{-1}): 1520 (s), 1352 (vs), 850 (s), 767 (m), 678 (m), 491 (w). UV – vis (THF): λ_{max} (ε) 474 nm (1550 M^{-1} cm^{-1}), 302 nm (22000 M^{-1} cm^{-1}).

Crystals of **1-(methyl 4-chlorobenzoate)$_2$** were obtained by dissolving 50 mg (0.053 mmol) of **1** in 3 mL of benzene. 100 mg (0.58 mmol) of methyl 4-chlorobenzoate were dissolved in the solution and the solvent was allowed to evaporate at room temperature under a nitrogen atmosphere. IR (solid in Parabar 10,312 oil, cm^{-1}): 1711 (m), 1558 (m), 1416 (vs), 1293 (s), 1088 (s), 845 (s), 757 (vs), 678 (m). UV – vis (PhMe): λ_{max} (ε) 454 nm (2350 M^{-1} cm^{-1}), 316 nm (20000 M^{-1} cm^{-1}).

Crystals of **1-NMP$_2$** were obtained by dissolving 50 mg (0.053 mmol) of **1** in 3 mL of THF. 1 mL of NMP was added and the solvent was allowed to evaporate at room temperature under a nitrogen atmosphere. IR (solid in Parabar 10,312 oil, cm^{-1}): 1520 (s), 1352 (vs), 850 (s), 767 (m), 678 (m), 491 (w). UV – vis (PhMe): λ_{max} (ε) 468 nm (1000 M^{-1} cm^{-1}), 301 nm (21000 M^{-1} cm^{-1}).

Crystals of **1 −TMEDA** were obtained by dissolving 50 mg (0.053 mmol) of **1** in 3 mL of THF. 1 mL of TMEDA was added and the solvent was allowed to evaporate at room temperature under a nitrogen atmosphere. IR (solid in Parabar 10,312 oil, cm^{-1}): 1520 (s), 1352 (vs), 850 (s), 767 (m), 678 (m), 491 (w). UV – vis (90/10 THF/TMEDA): λ_{max} (ε) 509 nm (1390 M^{-1} cm^{-1}), 317 nm (19000 M^{-1} cm^{-1}).

2.3. Synthesis and characterization of $Fe(^{Ar}acac)_2Cl$ (2)

A 100 mL schlenk flask was charged with 0.330 g (2.04 mmol) of $FeCl_3$, 2.000 g (4.54 mmol) of ^{Ar}acac-H and 50 mL of anhydrous benzene under a nitrogen atmosphere. The flask and its contents were removed from the glovebox and heated at 60 °C for 24 h. Evolved HCl was periodically flushed using nitrogen and a positive pressure. The Schlenk flask was returned to a nitrogen atmosphere glovebox and its contents filtered to collect unreacted $FeCl_3$. The filtrate's solvent was removed in vacuo and hexanes were added to remove unreacted ^{Ar}acac-H. The resulting mixture was filtered, dried and 1.764 g (89 %) of **2** was collected. Crystals of **2** were twinned. IR (solid in Parabar 10,312 oil, cm^{-1}): 1531 (vs), 1349 (vs), 846 (s), 764 (m), 678 (m), 496 (w). UV – vis (THF): λ_{max} (ε) 443 nm (2900 M^{-1} cm^{-1}). Anal. Calcd for $FeC_{62}H_{70}O_4Cl$: C, 76.73; H, 7.27; Found: C, 76.23; H, 7.35.

2.4. Synthesis and characterization of $[Fe(^{Ar}acac)(THF)_2]_2(\mu\text{-}OTf)_2$ (3)

A THF solution of $Fe(OTf)_2$ was prepared by addition of 134 mg AgOTf (0.52 mmol) and 33 mg $FeCl_2$ (0.26 mmol) and filtered to remove the precipitated AgCl. To this solution was added to 250 mg **1** (0.265 mmol) in THF and stirred for 12 h. The purple solution was cooled to room temperature and concentrated under vacuum. Purple crystals of **3** formed overnight to yield 254 mg of **3** (62 %). The THF and triflate moieties were disordered in the crystal lattice. Removal of THF from these crystals resulted in formation of **1** and insoluble solid, complicating further characterization of **3**.

2.5. Synthesis and characterization of $[Fe(^{Ar}acac)(Mes)]_2$ (4)

To a 20 mL scintillation vial with a PTFE coated stir bar, 0.265 g (0.901 mmol) of $Fe(mes)_2$ was dissolved in ~ 3 mL of toluene and the solution was frozen. 0.363 g (0.824 mmol) of ^{Ar}Acac-H was added to the solution upon thawing and stirred for 30 min. The resulting mixture was refrozen, and cold pentanes were layered upon the frozen toluene layer and stored at − 30 °C. After 48 h, $[Fe(^{Mes,tBu}Acac)Mes]_2$ was collected as a crystalline solid via filtration and dried under vacuum. Yield 0.480 g (47 %). Two molecules of toluene were present in the crystal lattice.

2.6. General catalytic procedure

A 20 mL scintillation vial was charged with 7 mL of anhydrous THF, 0.70 mL of *N*-methylpyrrolidine (NMP) and a PTFE coated stir bar. To the mixture, 0.200 g (1.17 mmol) of methyl 4-chlorobenzoate and 5.86 x 10^{-2} mmol of iron precatalyst (5 mol %) was added and chilled in a − 35 °C freezer for at least 1 h. The mixture was removed from the freezer and 0.80 mL of 2.0 M hexyl magnesium chloride in diethyl ether (1.36 mmol) was added dropwise with stirring. After the allotted time of stirring, the reaction was removed from the glovebox and diluted with ~ 10 mL of diethyl ether and quenched with 20 mL of 1 M HCl. The organics were extracted into diethyl ether and the organic layer was concentrated down to yield the product as an oil.

3. Results and discussion

3.1. Synthesis, characterization and catalysis using iron bis-metalated by acacs

Syntheses of Fe $(^{Ar}Acac)_2$ (**1**) and $Fe(^{Ar}Acac)_2Cl$ (**2**) were achieved by salt metathesis from the corresponding $FeCl_2$ and $FeCl_3$ precursors with $K(^{Ar}acac)$ with Fe^{2+} and $H(^{Ar}acac)$ with Fe^{3+} (Scheme 1). In the presence of THF, **1** converts to $Fe(^{Ar}Acac)_2(THF)_2$ (**1-THF$_2$**), which adopts a planar configuration of ^{Ar}acac ligands and a trans configuration of the THF ligands (Figs. S1 through S3). Of note is the lack of tris-metalation of acac ligands, leaving two and one open coordination sites in complexes **1** and **2**, respectively. Magnetic susceptibility measurements (Evans' method) of complexes **1** and **3** show a μ_{eff} of 4.9 and 6.0 Bohr magnetons, respectively, indicating these complexes are high-spin Fe^{II} and Fe^{III} species in solution. In addition to **1-THF$_2$**, **1** readily forms adducts with many solvents and substrate, including the bis-*N*-methyl pyrrolidine (NMP), bis(methyl 4-chlorobenzoate), and tetramethylethylenediamine (TMEDA) adducts (Fig. S5, S6, and S7). These structures demonstrate the diversity of substrate binding possible through the two open coordination sites on complex **1**.

The electrochemical behavior of compounds **1-THF$_2$** and **2** was then probed (Fig. 1). The cyclic voltammogram of **1–THF$_2$** shows a quasi-reversible oxidation event centered at − 297 mV, which is assigned as $Fe^{II/III}$ or **1** / **1**$^+$. Conversely, reduction of **2** requires a more negative reduction potential, with a peak observed at − 1429 mV vs. Fc/Fc^+. A new oxidation is subsequently observed, coinciding with the oxidation of **1–THF$_2$**, but the reduction wave at − 468 mV is not then observed. The electrochemistry of **2** is consistent with a $Fe^{III/II}$ reduction that is more negative due to the need to dissociate coordinated chloride ion from **2** to form **1**, followed by outer-sphere oxidation to form **1**$^+$.

Attempts to electrochemically reduce **1** and **2** to Fe^I were unsuccessful, with no reduction reaction observed out to –2.5 V. Attempts to chemically reduce **1** and **2** using cobaltocene, sodium mercury amalgam and potassium on graphite also do not result in an isolated Fe^I species. Attempts to oxidize **1-THF$_2$** in THF results in slow degradation of solvent, attributed to a ring opening reaction, as a thin film is observed on the working electrode after cycling. This is most likely due to the increased Lewis acidity of the metal center, which permits ring-opening polymerization of THF to occur at high enough voltages. When **1** is placed into 1,2-difluorobenzene, cyclic voltammetry reveals two quasi-reversible oxidation events with one at a much more positive po-

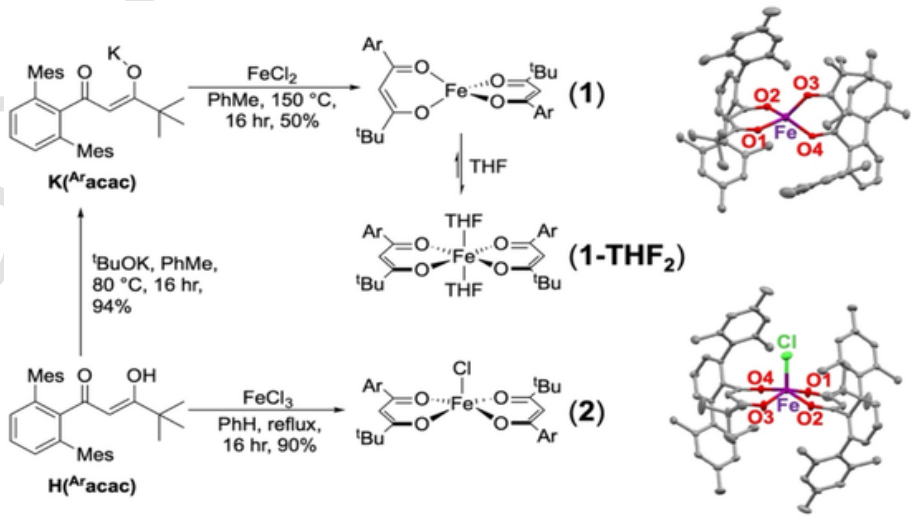

Scheme 1. Synthesis of compounds **1**, **1–THF$_2$** and **2**. (Right) Crystal structures of 1 and 2.

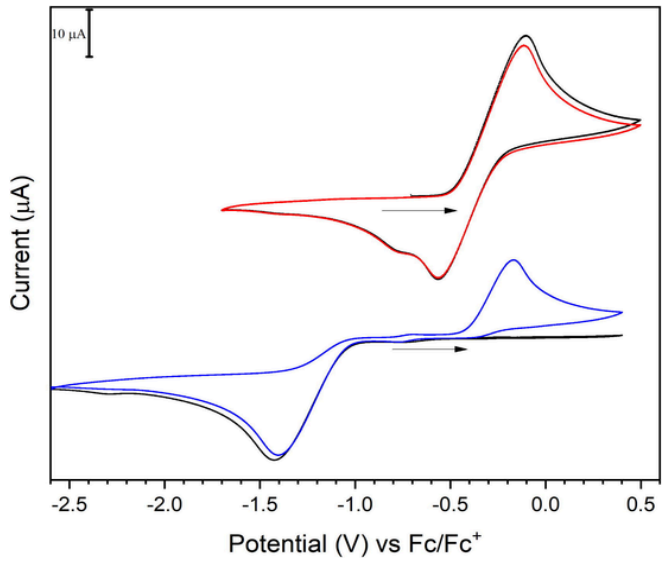

Fig. 1. Cyclic voltammogram of **1-THF$_2$** (red) and **2** (blue) at 100 mV s^{-1}, in 0.1 M TBAPF$_6$; the first scan is shown in black, and the second scan in color. ((Colour online.))

tential than attributed to the oxidation from Fe^{II} to Fe^{III} (Fig. 2). This appears to be an oxidation from Fe^{III} to Fe^{IV}, suggesting that Fe^{IV} might be a transiently accessible oxidation state for precatalyst **1**. Attempts to chemically oxidize **1** with XeF_2 were unsuccessful.

To determine the likely oxidation state of iron prior to catalysis, complexes **1-THF$_2$** and **2** UV–visible spectra were examined (Fig. 3). When **2** is exposed to hexyl-magnesium bromide the spectrum changes in less than one minute to align closely with **1-THF$_2$**. This spectrum remains constant for one hour in the presence of excess Grignard, suggesting that there is a rapid reduction of Fe^{III} to Fe^{II}, and that Fe^{II} is otherwise resistant to further reduction, metathesis, or nucleophilic substitution with the Grignard, absent of an electrophilic substrate. These observations are consistent with the prior electrochemical results, demonstrating that **2** is unable to be reduced from Fe^{II} to Fe^{I}.

Complexes **1-THF$_2$** and **2** were next examined as pre-catalysts in an iron-catalyzed Kumada cross-coupling reaction by measuring product yields at 15- and 60-minute time points (Table 1). Universally, **1-THF$_2$** and **2** proved to be less competent as a precatalyst than parent Fe(acac)$_3$. However, by altering additive components to enhance catalytic activity, several key observations can be made. First, the addition of $ZnBr_2$, which can act as an ^{Ar}acac ligand acceptor, slightly increases the yield for both Fe(acac)$_3$ and **1-THF$_2$**, even in the absence of NMP, though how many ligands zinc removes is left unclear. Second, TMEDA completely deactivates **1-THF$_2$** as a pre-catalyst, despite the fact that TMEDA is known to be an effective cosolvent or ligand in iron-catalyzed Kumada cross-coupling when using iron chloride salts [10, 32]. Instead, when TMEDA is used as a cosolvent, the only side product detected is the result of the Grignard reagent reacting with the ester carbonyl to generate the hexyl ketone. If acac ligands only serve to solubilize iron and completely dissociate before catalysis, then the presence of TMEDA should produce cross-coupled product. The fact that it does not produce cross-coupled product suggests that ^{Ar}acac remains coordinated during catalysis. Other studies utilizing Fe(acac)$_3$ report that the introduction of bidentate dimethoxyethane (DME) also attenuates catalysis [33].

UV–Visible spectroscopy studies of samples undergoing catalysis were next performed to investigate the electronic structure of the iron species during catalysis. During the catalytic reaction, a violet color similar to previous studies is observed, regardless of the pre-catalyst used [34]. When the reaction mixture is analyzed via UV–visible spectroscopy, the spectra of a reaction using either Fe(acac)$_3$ or **1-THF$_2$** as the pre-catalyst, both have a peak at 524 nm. This would suggest that both Fe(acac)$_3$ and **1-THF$_2$** are converted to the same active iron species. When **1-THF$_2$** and Fe(OTf)$_2$ are combined, the comproportiona-

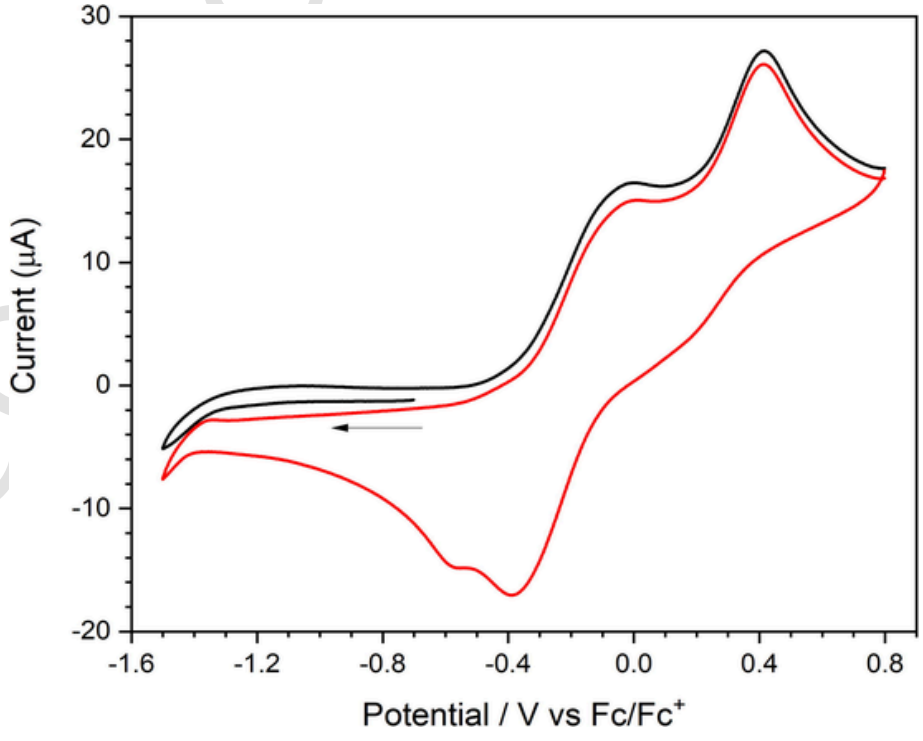

Fig. 2. Cyclic voltammogram of of **1** in 1,2-difluorobenzene (100 mV s^{-1}, 0.1 M TBAPF$_6$), first scan black, second scan red. ((Colour online.))

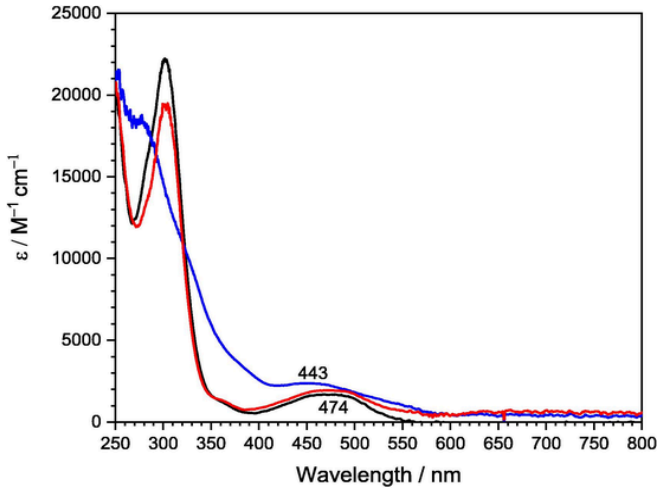

Fig. 3. UV–Vis spectra of **2** (blue) before exposure to Hexyl-Magnesium Bromide and < 1 min after exposure (red) and **1-THF$_2$** (black). ((Colour online.))

Table 1
Summary of first catalytic trials of **1-THF$_2$** and **2** compared against Fe(acac)$_3$

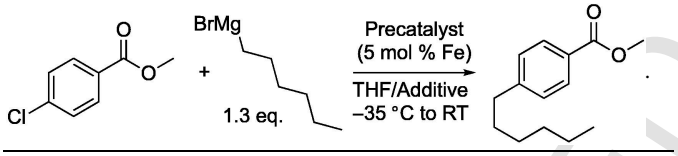

Pre-catalyst	Addition	Yield (%) at 15 min	Yield (%) at 60 min
Fe(acac)$_3$	NMP	92	93
Fe(acac)$_3$	None	43	48
Fe(acac)$_3$	ZnBr$_2$ (2 eq)	50	64
1-THF$_2$	NMP	49	50
1-THF$_2$	None	34	48
1-THF$_2$	TMEDA	<1	<1
1-THF$_2$	ZnBr$_2$ (1 eq)	50	53
2	NMP	36	44

tion product [Fe(^{Ar}acac)(THF)$_2$]$_2$(μ-OTf)$_2$ (**3**) is formed, which has the same 524 nm absorbance feature that is observed during catalysis (Fig. 4). One possible explanation for this overlap is that there is a species within the catalytic reaction that is similar in electronic structure to that of **3**. Although triflate anion is not present, bridging chloride ligands could also result in a structurally similar complex. Because this color is persistent in the catalytic reaction, this also suggests that there is a buildup of this halide bridged iron acac dimer that may act as a resting state for the catalyst.

Based on the catalytic enhancement using ZnBr$_2$, and the UV–Vis spectra and structural characterization of **3** (Fig. S9), it was hypothesized that Fe^{II} supported by a single acac ligand may be catalytically relevant. Two methods to synthesize iron supported by a single acac ligand proved successful: mixing **1-THF$_2$** with Fe(OTf)$_2$ to form **3** (Fig. 4) and by mixing 1.1 equivalents of Fe(Mes)$_2$ with H(^{Ar}acac) to generate [Fe(^{Ar}acac)]$_2$(μ-Mes)$_2$ (**4**) (Fig. 5). The X-ray crystal structure of **4** reveals pseudo-tetrahedral iron centers with bridging mesityl groups, and is the first example of an organoiron compound supported by acac ligands. Structural comparison of **4** with Fe$_2$Mes$_4$ shows a slightly elongated iron-iron distance of 2.64 Å vs. 2.617 Å, and the iron-carbon distances also show slight elongation (2.189 Å and 2.139 Å in **4** vs. 2.155 Å and 2.104 Å in Fe$_2$Mes$_4$).[35].

Evans' Method of **4** reveals a μ_{eff} of 1.70 ± 0.02 Bohr magnetons vs. 3.86 Bohr magnetons of Fe$_2$Mes$_4$, suggesting an increase in antiferromagnetic coupling between the two iron centers.[36] Curiously, the μ_{eff} of **4** is consistent with an S = ½ complex, suggesting that these iron dimers in solution may be the origin of the S = ½ complexes reported elsewhere in literature as evidence of Fe(I).[37] Cyclic voltammetry of **4** (Fig. S24) in THF suggests that oxidation of [Fe(^{Ar}acac)Mes]$_2$ degrades the dimer, because the current response decreases on the second scan. Because the oxidation potential is shifted to a more positive than **1-THF$_2$**, appearing at –187 mV vs. Fc/Fc$^+$ compared to the E$_{1/2}$ of **1-THF$_2$** at –333 mV, it suggests that **4** does not convert to **1-THF$_2$**.

With two routes to generating Fe(^{Ar}acac) dimers, the catalytic competency of these complexes was probed using the same Kumada coupling reaction between hexyl-magnesium bromide and methyl 4-chlorobenzoate. Additional conditions such as the removal of NMP as a cosolvent were examined, and several other iron pre-catalysts were tested as control experiments (Table 2). Fe^{II} triflate performs the worst, resulting in less than a 10 % yield of the desired product, though a mixture of **1-THF$_2$** and Fe(OTf)$_2$, which generates a solution of **3** *in situ* gives substantially better yield (88 %). In trials containing no NMP as a cosolvent, the mixture of **1-THF$_2$** and Fe(OTf)$_2$ performs better than pure **1-THF$_2$** with or without the addition of NMP as a cosolvent. More remarkable, however, is the sharp increase in catalytic efficacy of the catalyst upon the addition of NMP to **3**, with 15-minute yields reaching in excess of 80 % isolated yields and 60-minute yields approaching percent conversions rivaling the parent Fe(acac)$_3$. Fe(Mes)$_2$ performed remarkably better than Fe(OTf)$_2$ as a pre-catalyst, giving yields of approximately 60 % at both the 15- and 60-minute marks, demonstrating its superior performance when compared to **1-THF$_2$**. However, the acac supported **4** demonstrates improved yields compared to Fe(Mes)$_2$.

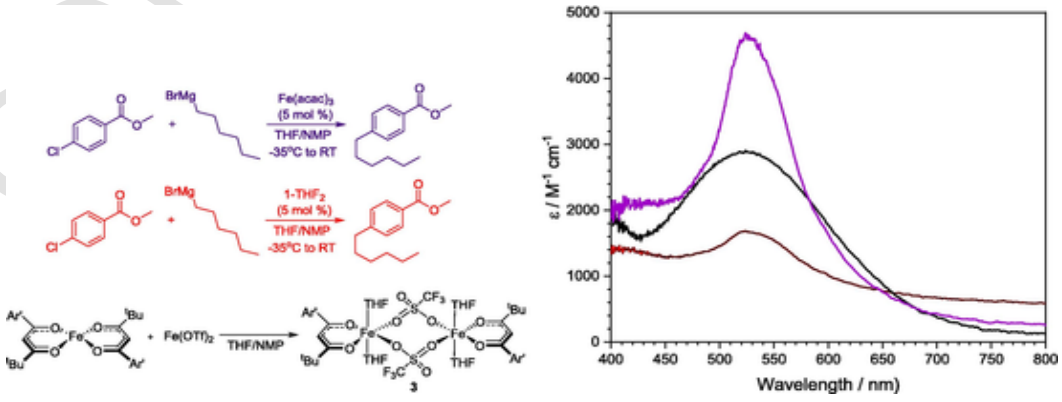

Fig. 4. UV–Vis spectra of Kumada coupling reaction in progress using Fe(acac)$_3$ precatalyst (violet), **1-THF$_2$** (red) and the UV–Visible spectrum of a mixture of **3** (black). ((Colour online.))

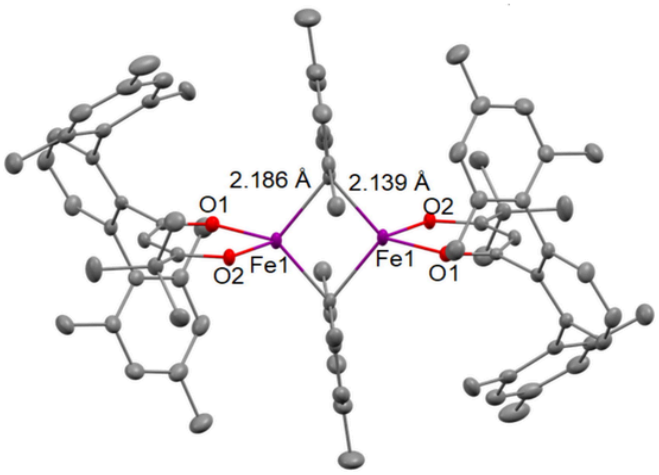

Fig. 5. X-Ray crystal structure of **4**.

Table 2
Summary of catalytic trials using ^{Ar}acacFe dimers **3** and **4** as pre-catalysts, as well as $Fe(OTf)_2$ and $Fe(Mes)_2$ controls

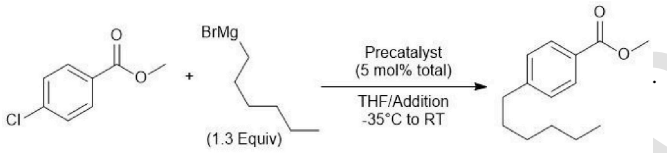

Pre-catalyst	Addition	Yield (%) at 15 min	Yield (%) at 60 min
3	None	60	64
3	NMP	81	88
4	None	65	87
4	NMP	75	90
$Fe(Mes)_2$	None	58	63
$Fe(OTf)_2$	NMP	5	8

Without NMP, **4** performs better than **1-THF_2** at both time intervals under all conditions. When NMP is included in the mixture, **4** reaches yields rivaling that of the parent $Fe(acac)_3$, similar to those of **3**. However, the yields are only reached after 60 min of reaction time, rather than the 92 % yield obtained after 15 min using $Fe(acac)_3$. A potential implication of this result is that the ligand sterics are impeding catalysis, potentially via steric crowding of the metal center or the slowing of a step during the catalytic process. Finally, the catalytic activity of the **4** in a non-coordinating solvent was investigated (not shown). No product was observed when using **4** as a pre-catalyst in toluene as a solvent without coordinating cosolvent additions. These results, in conjunction with the previous catalytic trials lead to several key hypotheses. First, iron supported by a single acac is most likely the relevant species in the context of catalysis. This is predicated upon the fact that not only does **4** prove to be nearly as effective as $Fe(acac)_3$, but **1-THF_2** performs better as pre-catalyst when mixed with $Fe(OTf)_2$ to generate the comproportionated product, **3.** In comparison, neither **1-THF_2** nor $Fe(OTf)_2$ are able to cross-couple as effectively as the mixture of the two. Second, a monomeric iron species is more likely to be relevant than a dimeric species, as **4** in toluene does not demonstrate any cross-coupling between electrophile and nucleophile. In this case the role of the coordinating solvent (THF or NMP) is to break up the iron dimer to re-enter the catalytic cycle.

Third, the steric bulk of the acac ligand appears to impact the reaction rate, based on yields at 15 and 60 min. The fact that **3** and **4** eventually reaches yields rivaling that of parent $Fe(acac)_3$, only on a longer time scale, suggests that while slower, they might remain active for longer time. Fourth, either the steric environment of larger acac ligands directly impedes catalysis or the catalyst activation via transmetalation of ^{Ar}acac from **1-THF_2** with the Grignard reagent is a slow step.

3.2. Computational studies

Using the hypotheses described above as guidance, DFT calculations were performed using acac-supported iron centers with simplified structures to reduce computation time. Experimental observations suggested two important factors to consider: Iron most likely starts in the + 2 oxidation state and a single acac ligand remains metalated throughout the cross-coupling. The $\Delta G_{reaction}$ of several reactions involving the geometry optimized structures were investigated, using a conductor-like screening model (COSMO) to act as a solvent environment (Table 3). It was found that the formation of a dimeric structure similar to **3** was favorable only when non-coordinating solvents were used. With solvents that were able to coordinate to iron, it was found that NMP binds more favorably to iron compared to THF by 1.2 kcal/mol. This may elucidate the role of NMP in iron-catalyzed Kumada coupling, as **4** does not afford cross-coupled product in the absence of coordinating solvents, suggesting that the dissociation of the dimer is most likely necessary for catalysis to occur.

A transition state scan using the nudged elastic band (NEB) method to find a minimum energy path (MEP) between a simplified version of the reactant and product states gave the an energy profile with two transition states and an intermediate of lower energy than the starting material (Fig. S25) [38,39]. The geometries of the transition states and intermediates were then optimized in the quintet and triplet spin state and plotted against the lowest energy geometry of the starting material (Fig. 6). Notably, an intermediate energy minimum was found along the MEP that suggests the existence of a five-coordinate Fe^{IV} intermediate during the catalytic cycle.

The first transition state can be described as an oxidative addition with a barrier of only a few kcal/mol, and the single imaginary frequency of the transition state involves a stretch of the C–Cl bond as it coordinates side-on to the Fe. The five-coordinate intermediate Fe(acac)Cl(Et)(Ar) (**5**) was found to be most stable as a quintet ground state with very small amounts of spin-density is found on either the ethyl or phenyl moieties; however this does not preclude an alternate description as Fe^{II} coordinating to two organic radicals antiferromagnetically coupled to the iron [40]. We note that cyclic voltammetry of **1** suggests the transient ability to access an Fe^{IV} oxidation state, though this could also be explained through oxidation of each of the acac ligands rather than the Fe [41,42]. The second transition state also has a low energy barrier and can best be described as a reductive elimination of the organometallic ligands to form the C—C bonded product. The resulting Fe(acac)Cl could re-enter the cycle through transmetalation from a Grignard or dimerize to form a chloride-bridged complex analogous to **3**, which could act as a catalyst resting state. The final product is

Table 3
Gibbs Free Energies of Reactions used in computational analyses and their computed Gibbs Free Energies of reaction.

Reaction	Computed $\Delta G_{reaction}$ (kcal/mol)
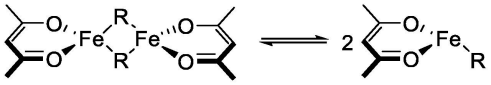	0.846
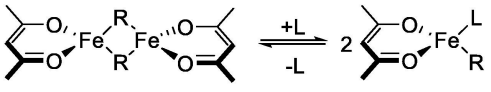	–25.8 (NMP) –24.6 (THF)
R = Ethyl L = NMP or THF	

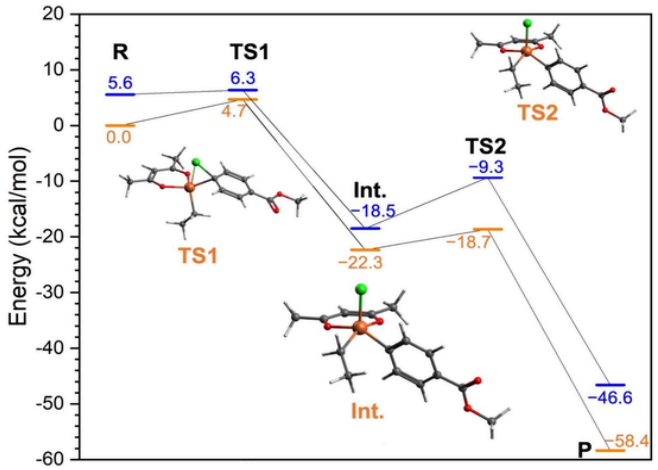

Fig. 6. Minimum energy pathway of the optimized quintet (orange) and triplet (blue) spin state geometries along the minimum energy path found during a transition state scan. Zero energy is defined by the reactants in the quintet state. ((Colour online.))

significantly lower in energy than the starting material, suggesting that the regeneration of the active organoiron species could be unfavorable with weaker nucleophiles than Grignard reagents.

The role of NMP as a solvent additive binding to iron was investigated by comparing the energies of in the starting material Fe(acac)Et, product Fe(acac)Cl, and intermediate **5** optimized with explicit NMP bound to the metal center. The binding of NMP and versus methyl 4-chlorobenzoate was first investigated, and found to be energetically disfavored by 9.5 kcal/mol. However, the optimized Fe^{IV} intermediate was found to be –15.44 kcal/mol lower in energy than the starting material, suggesting the possibility of associative substitution of methyl 4-chlorobenzoate with a concerted oxidative addition and dissociation of NMP. This is supported by the fact that **5** was calculated not to coordinate to NMP (Fig. 7). Moving from **5** to product geometries with NMP results in a $\Delta G_{reaction}$ of –45.3 kcal/mol as well, resulting in an overall $\Delta G_{reaction}$ of –60.8 kcal/mol demonstrating a similar energy profile of the minimum energy pathway without explicit solvent, which has an overall $\Delta G_{reaction}$ of –58.4 kcal/mol.

Finally, the role of NMP was further investigated using the Fe(acac)Cl product that results from reductive elimination. It was found that absent of solvent the dimer was preferred by 10.44 kcal/mol. However, the inclusion of NMP results in a favorable dissociation of the dimer into monomeric Fe(acac)Cl·NMP with a $\Delta G_{reaction}$ of –1.66 kcal/mol. This suggests that NMP could serve a similar role in both the generation of the active organoiron species and active iron chloride species, by preventing the formation of dimers in an off-cycle pathway or dissociating dimers that do form. In conjunction with the optimized intermediate, however, this appears to be NMP's only role, as the five-coordinate **5** appears to be preferred over a six-coordinate iron with NMP bound.

Studies using iron NacNac complexes in cross-coupling reactions have implicated the triplet spin state transition state, requiring a spin-cross over event from the quintet spin state to the triplet spin state [43]. However, throughout the calculated reaction pathway, the quintet spin state geometries all are lower in an energy than their triplet spin state counterparts, suggesting that this spin-crossover event is unnecessary with acac as an ancillary ligand. The first transition state in the triplet spin state is only 1.6 kcal/mol higher in energy than the quintet spin state, however, suggesting that spin-crossover events could be thermally accessible. In the event of a spin-crossover event occurring, catalysis may still proceed, as the triplet spin-state still represents a lower energy pathway relative to the rate determining step of oxidative addition. The ability of simple iron salts like iron-acac to have a higher density of states [44] (e.g. two accessible spin states throughout the catalytic cycle) may be the origin of iron's rapid coupling in Kumada cross-coupling reactions.

These results suggest that the most likely mechanism evokes a similar scheme to existing palladium and platinum cross coupling reactions while having a few key differences. The first step is the removal of a acac ligands via transmetalation reactions with the Grignard to form an organoiron(II) species supported by one acac ligand. Next, oxidative addition of the aryl chloride forms a nominal Fe^{IV} species **5** with the aryl, chloro and R group all bound to the iron center. Reductive elimination forms the new Ar–R bond and generating an Fe^{II}(acac)Cl species. Transmetalation with Grignard would reform the active Fe^{II}–R species, continuing the cycle (Scheme 2). Off-cycle pathways represented by the formation of dimers would be dissociated by the inclusion of NMP in the reaction mixture. This mechanism differs from traditional palladium-catalyzed Kumada cross-coupling reactions in that there is not an intervening transmetalation reaction after oxidative addition. Instead,

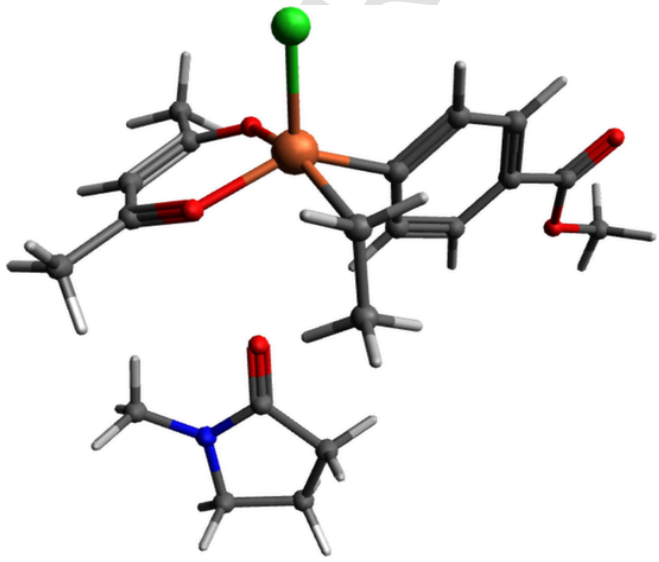

Fig. 7. Calculated geometry of **5** with an explicit NMP molecule included.

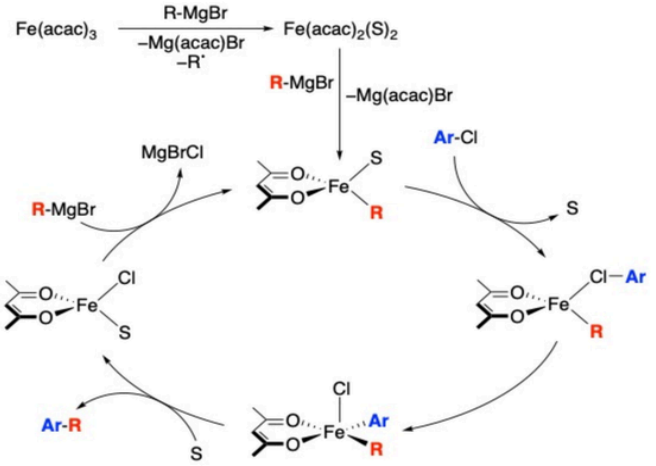

Scheme 2. Proposed catalytic cycle for $Fe(acac)_3$-catalyzed cross-coupling reaction based on experimental and computational results.

the first step is a transmetalation step that produces an organoiron species, and oxidative addition followed by reductive elimination occurs to generate the new C—C bond. Additionally, unlike the singlet spin state, closed-shell palladium-catalyzed cross-coupling, iron prefers an open shell, high spin metal manifold. This manifold which has been implicated as the preferred spin state of d^6 Fe(II) metal complexes in cross-coupling reactions, demonstrating why the use of phosphine and even NacNac ligands leads to lower yields or longer reaction times than reactions utilizing parent $Fe(acac)_3$ [45].

4. Conclusions

The Kumada coupling reaction of Methyl 4-chlorobenzoate and hexyl magnesium bromide have been used to serve as a model reaction to explore the catalysis of novel, sterically hindered iron acac complexes, enabling us to probe potential mechanistically relevant intermediates. Additionally, we have isolated the first examples of organoiron acacs. Compounds **1–4** proved to act as pre-catalysts, with the mono-acac dimers **3** and **4** approaching similar efficacy as the parent $Fe(acac)_3$.

While the identity of the active iron species in the catalytic process remains unknown, this work suggests a few possibilities. The iron pre-catalysts demonstrate resistance to electrochemical reduction, suggesting a Fe^{I} and lower oxidation states are unlikely present prior to catalysis. UV–Visible spectroscopy suggests some dimeric Fe^{II} species are present during catalysis. This, in conjunction with our computational results demonstrating that the formation of monomers is more favorable over dimers, suggests that the dimeric species is a resting state or an off-cycle pathway. Additionally, this offers an explanation as to why NMP has been shown to be an effective co-solvent in these types of Kumada cross-couplings, as it serves to dissociate and dimers that may form.[36] Our catalysis studies demonstrate that iron complexes supported by a single acac are more competent pre-catalysts than bis-acac iron complexes, suggesting that iron centers supported by a single acac ligand are the active species in catalysis. Additionally, the computational results support a mechanism involving an oxidative addition to Fe(acac)R to form an intermediate Fe^{IV} complex **5**, followed by quick reductive elimination to Fe^{II} to form the new C—C bond. A high valent iron complex could explalin why this reaction favors aryl-choride substrates over bromides and iodides, since the latter could more favorably form halogen radicals rather than support product formation.

The pyramidal geometry of **5** may shed light on NacNac-supported iron pre-catalysts' inability to match $Fe(acac)_3$ in product yield. In prior studies, a sterically encumbered NacNac demonstrates a poorer yield to $Fe(acac)_3$ using the same electrophile and nucleophile used in this studies [16]. The nitrogen-bound aryl groups sterically crowd the iron center, particularly within the NacNac plane, inhibiting oxidative addition or association of the aryl electrophile to Fe^{IV} that prefers a square pyramidal geometry. In contrast, the ^{Ar}acac ligand utilized does not have as much steric crowding around the metal center, leading to higher yields when using mono-acac supported iron centers. However, the bulkiness of this ligand slows the rate of activation of **1** via transmetalation of the ligand with the Grignard, causing it to be a less effective supporting ligand than parent acetylacetonate.

CRediT authorship contribution statement

Steven J. Scappaticci: Writing – original draft, Methodology, Investigation, Formal analysis. **Aaron S. Crossman:** Writing – original draft, Investigation, Formal analysis, Data curation. **Alec T. Larson:** Investigation. **Franklin D.R. Maharaj:** Investigation. **Eser S. Akturk:** Supervision, Methodology, Investigation. **Michael P. Marshak:** Writing – review & editing, Writing – original draft, Visualization, Supervision, Resources, Project administration, Methodology, Investigation, Funding acquisition, Conceptualization.

Declaration of competing interest

The authors declare the following financial interests/personal relationships which may be considered as potential competing interests: Michael Marshak reports financial support was provided by National Science Foundation. Michael Marshak has patent #US9676693B2 issued to Michael Marshak. If there are other authors, they declare that they have no known competing financial interests or personal relationships that could have appeared to influence the work reported in this paper.

Data availability

Data will be made available on request.

Acknowledgements

The research presented was funded by the National Science Foundation under Grant No. 2155227. The views and opinions of the authors expressed herein do not necessarily state or reflect those of the United States Government or any agency thereof. M.P.M would like to thank Prof. Peter Wolczanski for his inspiring use of bulky siloxide ligands to elucidate organometallic mechanisms and for his compelling insights on formal oxidation states in organometallics.

Appendix A. Supplementary data

Supplementary data to this article can be found online at https://doi.org/10.1016/j.poly.2024.117027.

References

[1] R.J.P. Corriu, J.P. Masse, Activation of Grignard reagents by transition-metal complexes. a new and simple synthesis of trans-stilbenes and polyphenyls, J. Chem. Soc. Chem. Commun. (1972) 144a, https://doi.org/10.1039/c3972000144a.
[2] K. Tamao, K. Sumitani, M. Kumada, Selective carbon-carbon bond formation by cross-coupling of Grignard reagents with organic halides. Catalysis by nickel-phosphine complexes, J. Am. Chem. Soc. 94 (1972) 4374–4376, https://doi.org/10.1021/ja00767a075.
[3] M. Tamura, J.K. Kochi, Vinylation of Grignard reagents. Catalysis by iron, J. Am. Chem. Soc. 93 (1971) 1487–1489, https://doi.org/10.1021/ja00735a030.
[4] A. Fürstner, Base-metal catalysis marries utilitarian aspects with academic fascination, Adv. Synth. Catal. 358 (2016) 2362–2363, https://doi.org/10.1002/adsc.201600729.
[5] B.D. Sherry, A. Fürstner, The promise and challenge of iron-catalyzed cross coupling, Acc. Chem. Res. 41 (2008) 1500–1511, https://doi.org/10.1021/ar800039x.
[6] T.L. Mako, J.A. Byers, Recent advances in iron-catalysed cross coupling reactions and their mechanistic underpinning, Inorg. Chem. 3 (2016) 766–790, https://doi.org/10.1039/C5QI00295H.
[7] B. Scheiper, M. Bonnekessel, H. Krause, A. Fürstner, Selective iron-catalyzed cross-coupling reactions of grignard reagents with enol triflates, acid chlorides, and dichloroarenes, J. Org. Chem. 69 (2004) 3943–3949, https://doi.org/10.1021/jo0498866.
[8] A. Fürstner, Iron catalysis in organic synthesis: a critical assessment of what it takes to make this base metal a multitasking champion, ACS Cent. Sci. 2 (2016) 778–789, https://doi.org/10.1021/acscentsci.6b00272.
[9] J.K. Kochi, Electron-transfer mechanisms for organometallic intermediates in catalytic reactions, Acc. Chem. Res. 7 (1974) 351–360, https://doi.org/10.1021/ar50082a006.
[10] A. Fürstner, R. Martin, H. Krause, G. Seidel, R. Goddard, C.W. Lehmann, Preparation, structure, and reactivity of nonstabilized organoiron compounds. implications for iron-catalyzed cross coupling reactions, J. Am. Chem. Soc. 130 (2008) 8773–8787, https://doi.org/10.1021/ja801466t.
[11] S.L. Daifuku, M.H. Al-Afyouni, B.E.R. Snyder, J.L. Kneebone, M.L. Neidig, A combined mössbauer, magnetic circular dichroism, and density functional theory approach for iron cross-coupling catalysis: electronic structure, in situ formation, and reactivity of iron-mesityl-bisphosphines, J. Am. Chem. Soc. 136 (2014) 9132–9143, https://doi.org/10.1021/ja503596m.
[12] S.L. Daifuku, J.L. Kneebone, B.E.R. Snyder, M.L. Neidig, Iron(II) active species in iron-bisphosphine catalyzed kumada and suzuki-miyaura cross-couplings of phenyl nucleophiles and secondary alkyl halides, J. Am. Chem. Soc. 137 (2015) 11432–11444, https://doi.org/10.1021/jacs.5b06648.
[13] V.E. Fleischauer, S.B. Muñoz III, P.G.N. Neate, W.W. Brennessel, M.L. Neidig, NHC and nucleophile chelation effects on reactive iron(ii) species in alkyl–alkyl cross-coupling, Chem. Sci. 9 (2018) 1878–1891, https://doi.org/10.1039/

C7SC04750A.
[14] G. Bauer, M.D. Wodrich, R. Scopelliti, X. Hu, Iron pincer complexes as catalysts and intermediates in alkyl-aryl kumada coupling reactions, Organometallics. 34 (2015) 289–298, https://doi.org/10.1021/om501122p.
[15] M.L. Neidig, S.H. Carpenter, D.J. Curran, J.C. DeMuth, V.E. Fleischauer, T.E. Iannuzzi, P.G.N. Neate, J.D. Sears, N.J. Wolford, Development and evolution of mechanistic understanding in iron-catalyzed cross-coupling, Acc. Chem. Res. 52 (2019) 140–150, https://doi.org/10.1021/acs.accounts.8b00519.
[16] K. Ding, F. Zannat, J.C. Morris, W.W. Brennessel, P.L. Holland, Coordination of N-methylpyrrolidone to iron(II), J. Organomet. Chem. 694 (2009) 4204–4208, https://doi.org/10.1016/j.jorganchem.2009.09.005.
[17] P.P. Power, Stable two-coordinate, open-shell (d 1 –d 9) transition metal complexes, Chem. Rev. 112 (2012) 3482–3507, https://doi.org/10.1021/cr2004647.
[18] E.S. Akturk, S.J. Scappaticci, R.N. Seals, M.P. Marshak, Bulky β-diketones enabling new lewis acidic ligand platforms, Inorg. Chem. 56 (2017) 11466–11469, https://doi.org/10.1021/acs.inorgchem.7b02077.
[19] S.M. Krajewski, A.S. Crossman, E.S. Akturk, T. Suhrbier, S.J. Scappaticci, M.W. Staab, M.P. Marshak, Sterically encumbered β-diketonates and base metal catalysis, Dalton Trans. 48 (2019) 10714–10722, https://doi.org/10.1039/C9DT02293G.
[20] A.S. Crossman, A.T. Larson, J.X. Shi, S.M. Krajewski, E.S. Akturk, M.P. Marshak, Synthesis of sterically hindered β-diketones via condensation of acid chlorides with enolates, J. Org. Chem. 84 (2019) 7434–7442, https://doi.org/10.1021/acs.joc.9b00433.
[21] E.J. Hopkins, S.M. Krajewski, A.S. Crossman, F.D.R. Maharaj, L.T. Schwanz, M.P. Marshak, Group 4 organometallics supported by sterically hindered β -diketonates: group 4 organometallics supported by sterically hindered β -diketonates, Eur. J. Inorg. Chem. 2020 (2020) 1951–1959, https://doi.org/10.1002/ejic.202000135.
[22] A.T. Larson, A.S. Crossman, S.M. Krajewski, M.P. Marshak, Copper(II) as a platform for probing the steric demand of bulky β-diketonates, Inorg. Chem. 59 (2020) 423–432, https://doi.org/10.1021/acs.inorgchem.9b02721.
[23] A.S. Crossman, J.X. Shi, S.M. Krajewski, L.A. Maurer, M.P. Marshak, Synthesis, reactivity, and crystallography of a sterically hindered acyl triflate, Tetrahedron. (2021) 132308, https://doi.org/10.1016/j.tet.2021.132308.
[24] A.S. Crossman, M.P. Marshak, 1.11 - β-Diketones: Coordination and Application, in: E.C. Constable, G. Parkin, L. Que Jr (Eds.), Compr. Coord. Chem. III, Elsevier, Oxford, 2021: pp. 331–365. https://doi.org/10.1016/B978-0-08-102688-5.00069-6.
[25] A. Klose, E. Solari, C. Floriani, A. Chiesi-Villa, C. Rizzoli, N. Re, Magnetic properties diagnostic for the existence of Iron(II)-Iron(II) bonds in dinuclear complexes which derive from stepwise insertion reactions on unsupported iron-aryl bonds, J. Am. Chem. Soc. 116 (1994) 9123–9135, https://doi.org/10.1021/ja00099a030.
[26] J.R. Hagadorn, W.B. Que Lawrence, Tolman, A bulky benzoate ligand for modeling the carboxylate-rich active sites of non-heme diiron enzymes, J. Am. Chem. Soc. 120 (1998) 13531–13532, https://doi.org/10.1021/ja983333t.
[27] C.A. Brown, Saline hydrides and superbases in organic reactions. II. Facile reaction of potassium hydride with ketones. rapid, quantitative formation of potassium enolates from ketones via kaliation, J. Org. Chem. 39 (1974) 1324–1325, https://doi.org/10.1021/jo00923a042.
[28] D.F. Evans, 400. The determination of the paramagnetic susceptibility of substances in solution by nuclear magnetic resonance, J. Chem. Soc. Resumed. (1959) 2003–2005, https://doi.org/10.1039/JR9590002003.
[29] G.M. Sheldrick, SHELXT – integrated space-group and crystal-structure determination, Acta Crystallogr. Sect. Found. Adv. 71 (2015) 3–8, https://doi.org/10.1107/S2053273314026370.
[30] G.M. Sheldrick, Crystal structure refinement with SHELXL, Acta Crystallogr. Sect. C Struct. Chem. 71 (2015) 3–8, https://doi.org/10.1107/S2053229614024218.
[31] O.V. Dolomanov, L.J. Bourhis, R.J. Gildea, J.A.K. Howard, H. Puschmann, OLEX2: a complete structure solution, refinement and analysis program, J. Appl. Crystallogr. 42 (2009) 339–341, https://doi.org/10.1107/S0021889808042726.
[32] D. Noda, Y. Sunada, T. Hatakeyama, M. Nakamura, H. Nagashima, Effect of TMEDA on iron-catalyzed coupling reactions of ArMgX with alkyl halides, J. Am. Chem. Soc. 131 (2009) 6078–6079, https://doi.org/10.1021/ja901262g.
[33] G. Cahiez, H. Avedissian, Highly stereo- and chemoselective iron-catalyzed alkenylation of organomagnesium compounds, Synthesis. 1998 (1998) 1199–1205, https://doi.org/10.1055/s-1998-2135.
[34] A. Fürstner, A. Leitner, Iron-catalyzed cross-coupling reactions of alkyl-grignard reagents with aryl chlorides, tosylates, and triflates, Angew. Chem. Int. Ed. 41 (2002) 609–612, https://doi.org/10.1002/1521-3773(20020215)41:4<609::AID-ANIE609>3.0.CO;2-M.
[35] H. Müller, W. Seidel, H. Görls, Zur chemie des dimesityleisens: VI. die struktur von tetramesityldieisen, J. Organomet. Chem. 445 (1993) 133–136, https://doi.org/10.1016/0022-328X(93)80198-K.
[36] R. Prabha, U.S. Nandi, Metal chelates in vinyl polymerization. I. Ferric dipivaloylmethide as an initiator, J. Polym. Sci. Polym. Chem. Ed. 15 (1977) 1973–1981, https://doi.org/10.1002/pol.1977.170150817.
[37] C.J. Adams, R.B. Bedford, E. Carter, N.J. Gower, M.F. Haddow, J.N. Harvey, M. Huwe, M.Á. Cartes, S.M. Mansell, C. Mendoza, D.M. Murphy, E.C. Neeve, J. Nunn, Iron(I) in negishi cross-coupling reactions, J. Am. Chem. Soc. 134 (2012) 10333–10336, https://doi.org/10.1021/ja303250t.
[38] G. Henkelman, H. Jónsson, Improved tangent estimate in the nudged elastic band method for finding minimum energy paths and saddle points, J. Chem. Phys. 113 (2000) 9978–9985, https://doi.org/10.1063/1.1323224.
[39] H. Jonsson, G. Mills, K.W. Jacobsen, CHAPTER 16 Nudged elastic band method for nding minimum energy paths of transitions, (n.d.) 20.
[40] P.T. Wolczanski, Flipping the oxidation state formalism: charge distribution in organometallic complexes as reported by carbon monoxide, Organometallics. 36 (2017) 622–631, https://doi.org/10.1021/acs.organomet.6b00820.
[41] M.P. Marshak, M.B. Chambers, D.G. Nocera, Cobalt in a Bis-β-diketiminate environment, Inorg. Chem. 51 (2012) 11190–11197, https://doi.org/10.1021/ic301970w.
[42] M. Gotthold Vinum, L. Voigt, S.H. Hansen, C. Bell, K. Marie Clark, R. Wugt Larsen, K.S. Pedersen, Ligand field-actuated redox-activity of acetylacetonate, Chem. Sci. 11 (2020) 8267–8272, https://doi.org/10.1039/D0SC01836H.
[43] R.B. Bedford, How low does iron go? chasing the active species in fe-catalyzed cross-coupling reactions, Acc. Chem. Res. 48 (2015) 1485–1493, https://doi.org/10.1021/acs.accounts.5b00042.
[44] K.F. Hirsekorn, E.B. Hulley, P.T. Wolczanski, T.R. Cundari, Olefin substitution in (silox)3M(olefin) (silox = tBu3SiO; M = Nb, Ta): the role of density of states in second vs third row transition metal reactivity, J. Am. Chem. Soc. 130 (2008) 1183–1196, https://doi.org/10.1021/ja074972j.
[45] A. Nandy, H.J. Kulik, Why conventional design rules for C-H activation fail for open-shell transition-metal catalysts, ACS Catal. 10 (2020) 15033–15047, https://doi.org/10.1021/acscatal.0c04300.